Dalton Transactions

PAPER

View Article Online
View Journal | View Issue

Cite this: *Dalton Trans.*, 2017, **46**, 5680

Modulation of the CO_2 fixation in dinickel azacryptands†

F. Möller,[a] L. Castañeda-Losada,[a] J. R. C. Junqueira,[a] R. G. Miller,[a] M. L. Reback,[a] B. Mallick,[a] M. van Gastel*[b] and U.-P. Apfel*[a]

Received 30th November 2016,
Accepted 4th February 2017

DOI: 10.1039/c6dt04527h

rsc.li/dalton

While bimetallic azacryptands are known to selectively coordinate CO_2, there is little knowledge on how different substitution patterns of the azacryptand cage structure influence CO_2 coordination. Stopped-flow UV-vis spectroscopy, electrochemical analysis and DFT calculations were performed on a series of dinickel azacryptands and showed different rates of CO_2 coordination to the complexes. We herein present data showing that the different flexibility of the azacryptands is directly responsible for the difference in the CO_2 uptake capability of dinickel azacryptand complexes.

Introduction

The fixation and utilization of CO_2 as a C1-building block is an important research field towards the recycling of the potent greenhouse gas CO_2.[1] While enzymes like CO-dehydrogenases[9] and ureases[10] allow selective CO_2 fixation under mild and aqueous conditions,[7,8] they are not cost effective for industrial use. Therefore, it is vital to develop materials that are as selective and efficient as enzymes but at a much lower cost. Indeed a number of synthetic approaches for the fixation and transportation of CO_2 have been reported, such as metal organic frameworks (MOFs),[2] covalent organic frameworks (COFs)[3,4] or even inorganic carbonates.[5,6] Although they show promising properties, most of them have low selectivity towards CO_2 in the presence of other atmospheric gases and also low stability in the presence of moisture.[7,8] Cryptands, such as bis-Tren azacryptands (Tren = tris(2-aminoethyl)amine), have been shown to allow selective fixation and transportation of small molecules (*e.g.* bicarbonates, azides or thiocyanates).[9–13] By using cryptands, nowadays frequently used for anion recognition as well as in metal chelation, an attempt for a comparable strategy for CO_2 fixation was made.[14] The stability and selectivity of the resulting compounds for the fixation of small molecules depend on the cage size as well as on the effective size of the small molecules.[9,10,13,15–18] As a result, the uptake and binding properties of small molecules (*e.g.* halogenides and pseudohalogenides) can be selectively tuned by increasing the size of the cryptand and/or altering the binding motifs. The size of the binding cavity of cryptands for a potential small molecule to enter can be rationally designed by using different linker molecules connecting both Tren-moieties (Scheme 1).[19] Along this line, Nelson *et al.* recently showed crystallographic evidence for different CO_2 coordination in dicobalt-azacryptand complexes.[20] While $[Co_2L_A^{Fur}](ClO_4)_2$ reveals a short Co–Co distance of 4.2924(3) Å and a M–O_{CO_2} bond length of 2.145(9) Å, the Co–Co distance

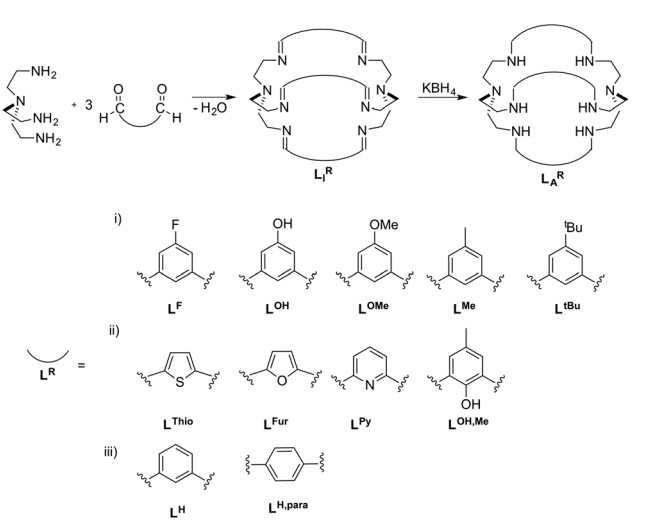

Scheme 1 Azacryptands L_A^R and imines L_I^R with different linker molecules L^R. The linkers are arranged according to their (i) different steric bulks on the central benzyl unit, (ii) capability to directly alter the electron density within the azacryptand cavity and (iii) different cage sizes.[5,14,15,17,20]

[a]*Inorganic Chemistry I/Bioinorganic Chemistry, Ruhr University Bochum, Universitätsstraße 150, 44801 Bochum, Germany. E-mail: ulf.apfel@rub.de*
[b]*Max-Planck-Institut für Chemische Energiekonversion, Stiftstraße 34-36, 45470 Mülheim, Germany*

†Electronic supplementary information (ESI) available: Synthesis and characterization of compounds, X-ray crystallographic analysis, UV-Vis spectra, SQUID and kinetic data. CCDC 1517780–1517787 and 1517950. For ESI and crystallographic data in CIF or other electronic format see DOI: 10.1039/c6dt04527h

in $[Co_2L_A^{H}](ClO_4)_2$ is significantly increased to 5.939(2) Å and the M–O_{CO_2} bond length is decreased to 1.920(6) Å. Mechanistic insight into the CO_2 fixation in $[Cu_2L_A^{H}](ClO_4)_3$ and $[Cu_2L_A^{H,para}](ClO_4)_3$ was provided by Chen as well as Mooney *et al.*, where they highlighted the necessity of an additional hydroxyl group on one metal site for successful CO_2 uptake.[19,21] Likewise, DFT-calculations were reported for $[Cu_2L_A^{Thio}]^{4+}$, $[Cu_2L_A^{H}]^{4+}$ and $[Cu_2L_A^{Fur}]^{4+}$, with the lowest energy barrier for CO_2 binding reported for $[Cu_2L_A^{Fur}]^{4+}$.[19] Notably, alteration of the linker not only had an effect on the substrate binding but also had a strong influence on the metal binding strength as was shown for $\mathbf{L_A^{Thio}}$, $\mathbf{L_A^{Fur}}$ and $\mathbf{L_A^{Py}}$.[22] We recently showed that $[Ni_2L_A^{H}](Cl)(ClO_4)_3$ is capable of performing rapid CO_2 uptake from air (k = 0.067 ± 0.005 M^{-1} s^{-1}) and was able to reversibly bind CO_2 by substitution with azides.[23] Furthermore, we could show that the azide ligand could be replaced by atmospheric CO_2 in a quasi-reversible process upon irradiation with UV light. Surprisingly, $[Ni_2L_A^{tBu}](Cl)(ClO_4)_3$ did not reveal any notable CO_2 fixation. Inspired by our initial results on the different binding capabilities of $[Ni_2L_A^{H}]^{4+}$ and $[Ni_2L_A^{tBu}]^{4+}$ as well as the opposing theoretical reports on altered CO_2 binding by varied linker moieties, we set out to further experimentally and theoretically elucidate the effects of linker variations in azacryptand cages on the CO_2 uptake capability and kinetics.

Results and discussion

Synthesis and characterization

The azacryptands $\mathbf{L_A^R}$ were synthesized *via* a two-step synthesis according to literature procedures (Scheme 1).[9,19,20,23–26] In a first step, [2 + 3]-Schiff-base condensation of the respective dialdehydes and Tren afforded the imines $\mathbf{L_I^R}$ in good yields (57–77%). The reaction of $\mathbf{L_I^R}$ with KBH_4 yielded the azacryptands $\mathbf{L_A^R}$ in good to excellent yields (66–99%). The molecular structures of the hexa-imines $\mathbf{L_I^F}$, $\mathbf{L_I^{OMe}}$ and $\mathbf{L_I^{Me}}$, and the hexa-amines $\mathbf{L_A^{Py}}$ and $\mathbf{L_A^{OH}}$ are presented in Fig. S1 and S2.† A simple way to investigate the influence of the linker molecule on the metal cryptand properties during CO_2 uptake is the application of the imine species $\mathbf{L_I^R}$ since they are structurally more rigid than their amine counterparts. We therefore attempted complex formation of the hexa-imines with $Ni(ClO_4)_2{\cdot}6H_2O$. The reaction solely afforded $\mathbf{[(Tren)Ni(CH_3CN)_2](ClO_4)_2}$ in 33% yield by a Ni-catalyzed imine hydrolysis in the presence of water of crystallization (Scheme 2).[27] The molecular structure was unequivocally confirmed by X-ray crystallography (Fig. S3†). Similar decomposition results were also observed for other hexa-imine azacryptands by ESI-MS. The only exception was $\mathbf{L_I^{OH,Me}}$, which afforded a mononuclear complex when reacted with $MnCl_2$; similar results are reported in the literature.[28]

Due to the instability of the imine complexes in the presence of moisture, we did not further investigate the imines towards the possibility of CO_2 coordination and instead focused on the hexa-amines $\mathbf{L_A^R}$ as ligands. The coordination

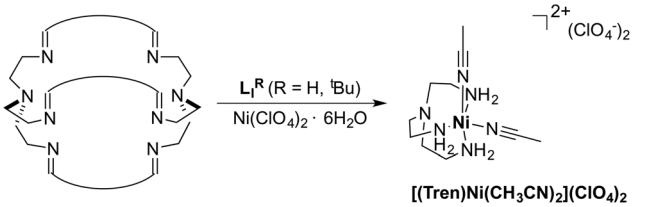

Scheme 2 Formation of $\mathbf{[(Tren)Ni(CH_3CN)_2](ClO_4)_2}$ through Ni-catalyzed imine-cleavage.

reactions of $\mathbf{L_A^R}$ with $Ni(ClO_4)_2{\cdot}6H_2O$ were performed under a nitrogen atmosphere to avoid any bicarbonate formation (Scheme 3). While the UV-vis spectra of $\mathbf{[Ni_2L_A^R](Cl)(ClO_4)_3}$ ($\mathbf{L_A^R}$ = $\mathbf{L_A^H}$, $\mathbf{L_A^F}$, $\mathbf{L_A^{OMe}}$ and $\mathbf{L_A^{Me}}$) showed absorption bands at ~390, 480, 560, and 620 nm, the spectra of $\mathbf{[Ni_2L_A^R](Cl)(ClO_4)_3}$ ($\mathbf{L_A^R}$ = $\mathbf{L_A^{tBu}}$, $\mathbf{L_A^{OH}}$, $\mathbf{L_A^{H,para}}$ and $\mathbf{L_A^{Fur}}$) solely revealed a broad band at ~580 nm containing a shoulder at lower wavelengths (Fig. 1, S4 and S5†). While a detailed band assignment has not been possible, recent crystallographic studies on $\mathbf{[Ni_2L_A^H](Cl)(ClO_4)_3}$ and $\mathbf{[Ni_2L_A^{tBu}](Cl)(ClO_4)_3}$ suggest an overall unchanged

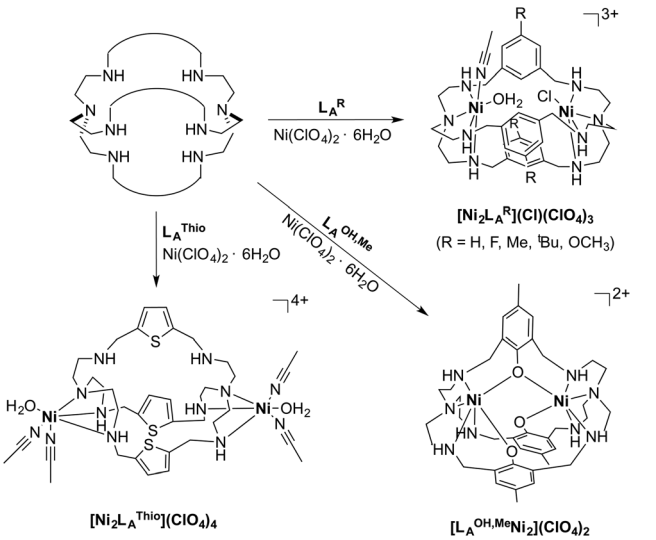

Scheme 3 Reaction of the azacryptands L_A^R with $Ni(ClO_4)_2{\cdot}6H_2O$.

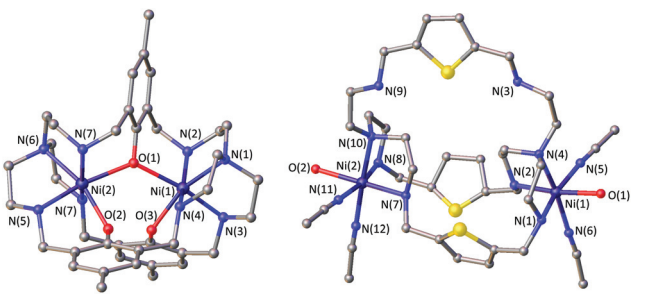

Fig. 1 Molecular structures of $[Ni_2L_A^{OH,Me}](ClO_4)_2$ (left) and $[Ni_2L_A^{Thio}](ClO_4)_4$ (right). Hydrogen atoms and counter ions were omitted for clarity.

shared structural motif of the above-mentioned complexes.[23] Likewise, ESI-MS experiments support a similar composition of the compounds by showing comparable mass patterns (Fig. S6†). Structural analysis revealed that one of the two Ni(II)-centers is coordinated by a water molecule and an acetonitrile, while the other is coordinated to a chloride.[23] Notably, different molecular assemblies were observed upon the reaction of $Ni(ClO_4)_2{\cdot}6H_2O$ with either $\mathbf{L_A^{Thio}}$ or $\mathbf{L_A^{OH,Me}}$. The molecular structure of $\mathbf{[Ni_2L_A^{OH,Me}](ClO_4)_2}$ (Fig. 1) reveals two octahedrally coordinated Ni-centers. Each Ni-center is surrounded by four nitrogen-donor atoms of the Tren-ligand with an average Ni–N distance of 2.14 Å. Additionally, one phenolate linker is coordinated in a μ^2-fashion, bridging both Ni-atoms with bonding distances of 2.164(2) [Ni(1)–O(1)] and 2.177(2) [Ni(2)–O(1)] Å. The coordination sphere of each Ni-center is completed by a non-bridging phenolate linker with Ni(1)–O(3) and Ni(2)–O(2) distances of 2.033(3) and 2.021(3) Å, respectively. While this compound appears to be a mixed valent Ni(II)/Ni(III)-species, its low synthetic yield (13%) stopped us from elucidating the exact electronic nature. It is possible that protonation of the ligand framework takes place to afford an all Ni(II)-species. Surprisingly, $\mathbf{L_A^{Thio}}$ revealed a different coordination behavior in the solid state where both Ni-atoms are coordinated on the outside of the cryptand cavity, as was reported for the structurally related complexes $[Cu_2L_A^{Thio}](O_3SOCF_3)_2$ and $[Ag_2L_A^{Thio}](ClO_4)_2$.[29] Each Ni(II)-center is octahedrally coordinated to only three N-donor atoms of the Tren-moiety as well as two additional acetonitriles and one water ligand. We assume that the different structure of $\mathbf{[Ni_2L_A^{Thio}](ClO_4)_4}$ compared to *e.g.* $\mathbf{[Ni_2L_A^{H}](Cl)(ClO_4)_3}$ can be explained by a different metal binding affinity and therefore an altered complex stabilization, as was reported by Nelson and co-workers.[22] We next investigated the CO_2 fixation behavior of all $\mathbf{[Ni_2L_A^{R}](Cl)(ClO_4)_3}$ complexes by UV-vis spectroscopy and ESI-MS. A clear change in the UV-vis spectra upon purging the $\mathbf{[Ni_2L_A^{R}](Cl)(ClO_4)_3}$ (R = H, F, OMe, Me and Fur) solutions with CO_2 is observed, showing a decrease in absorption intensity of the bands between 430–580 nm with the formation of an intense absorption band at about 610 nm (Fig. 2 and S4†). The amplitude of the absorption band as well as the disappearance of the original bands between 430–580 nm depends on the substitution pattern at the linker unit.

In analogy to our recent finding for $\mathbf{[Ni_2L_A^{H}](Cl)(ClO_4)_3}$, such changes can be attributed to the coordination of CO_2 within the cavity of the cryptand to afford a bicarbonate dinickel complex.[23] ESI-MS analysis further supports the fixation of either $^{12}CO_2$ or $^{13}CO_2$ for the reported complexes by the appearance of the $\mathbf{[Ni_2L_A^{R}(HCO_3)]}$ mass-peak (Fig. S7 and S8†).[23] Notably, while the color changes of the complexes upon reaction with CO_2 are usually unclear from dark to light blue, $\mathbf{[Ni_2L_A^{F}](Cl)(ClO_4)_3}$ reveals a distinct color change upon CO_2 fixation from blue to red (Fig. S9 and S10†). In contrast, no apparent changes could be observed for the complexes comprising the $\mathbf{L_A^{Thio}}$, $\mathbf{L_A^{OH}}$, $\mathbf{L_A^{Py}}$, or $\mathbf{L_A^{OH,Me}}$ moiety. Likewise, ESI-MS analysis solely revealed the mass peaks of the starting complexes. It can thus be assumed that these complexes do not possess the capability to fixate CO_2 under the described reaction conditions, although a small shift of the main band from 564 nm to 571 nm was observed in the UV-vis spectrum upon CO_2 addition to $\mathbf{[Ni_2L_A^{H,para}](Cl)(ClO_4)_3}$. ESI-MS showed a new mass-peak at m/z = 756, which clearly indicates a reaction of $\mathbf{[Ni_2L_A^{H,para}](Cl)(ClO_4)_3}$ to afford a new complex. This behavior can most likely be attributed to the formation of $\mathbf{[Ni_2L_A^{H,para}(CN)](ClO_4)_3}$ comprising a bridging CN^--ligand but no coordinated bicarbonate. Further evidence for the presence of a CN^- ligand was provided by IR spectroscopy showing a signal at 2022 cm^{-1} that can be assigned to a bridging CN^- moiety. A similar observation was recently reported for $[Cu_2L_A^{H,para}(CN)](ClO_4)_3$, which was obtained *via* C–C bond cleavage of a coordinated acetonitrile.[30]

Recent DFT calculations by Mooney *et al.* suggested an even better CO_2-fixation in $[Cu_2L_A^{Thio}]$ than in the respective $[Cu_2L_A^{H}]$ complex.[19] In contrast, $\mathbf{[Ni_2L_A^{Thio}](ClO_4)_4}$ does not perform any CO_2 uptake. Our finding is supported by a recent experimental investigation of Fabbrizzi and co-workers who report on the inability of $[Cu_2L_A^{Thio}](ClO_4)_3$ to bind the HCO_3^- anion.[15]

Kinetic analysis

To further evaluate the differences of the azacryptand platform we performed UV-vis stopped-flow investigations. We expected a significant alteration of the CO_2 uptake kinetics with different substitution patterns. The time-dependent absorption changes were measured at different temperatures (15–45 °C) and CO_2 concentrations. The obtained absorption changes were then fitted using a pseudo-first order equation of the type $A = A_0 \exp(-k_{obs}{\cdot}t)$ (A = absorbance, A_0 = initial absorbance, t = time in s) (Tables 1, S1–S3 and Fig. 3, S11†). The obtained data clearly demonstrate that the CO_2 uptake rate is dependent upon the substitution pattern of the dinickel aza-

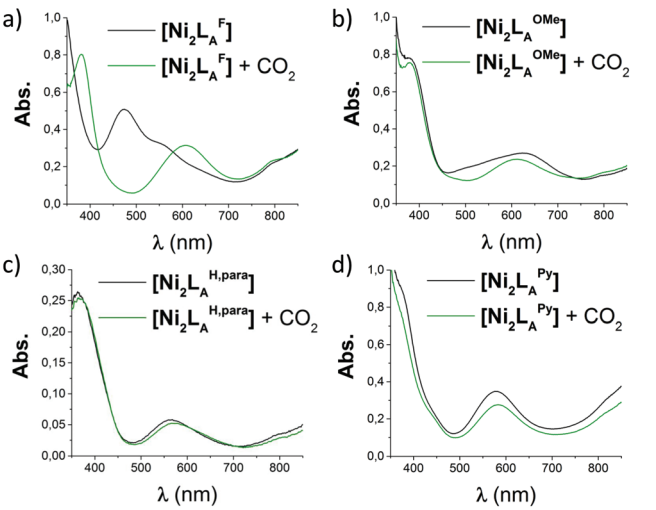

Fig. 2 UV-vis spectra (MeCN/MeOH 4 : 1, RT) of the reaction of $\mathbf{[Ni_2L_A^{R}](Cl)(ClO_4)_3}$ with CO_2: (a) $\mathbf{[Ni_2L_A^{F}]}$, (b) $\mathbf{[Ni_2L_A^{OMe}]}$, (c) $\mathbf{[Ni_2L_A^{H,para}]}$ and (d) $\mathbf{[Ni_2L_A^{Py}]}$.

Table 1 k_2 values obtained from the slope of the plot of k_{obs} *vs.* the CO_2 concentration at 298.15 K

$[Ni_2L_A^R]$	k_2 [M^{-1} s^{-1}]	$[Ni_2L_A^R]$	k_2 [M^{-1} s^{-1}]
L_A^H	$6.7 \times 10^{-2} \pm 5.0 \times 10^{-3}$	L_A^{Me}	$1.6 \times 10^{-2} \pm 1.1 \times 10^{-3}$
L_A^F	$2.0 \times 10^{-2} \pm 3.1 \times 10^{-3}$	L_A^{Fur}	$9.8 \times 10^{-4} \pm 1.1 \times 10^{-4}$
L_A^{OMe}	$1.9 \times 10^{-2} \pm 2.7 \times 10^{-3}$		

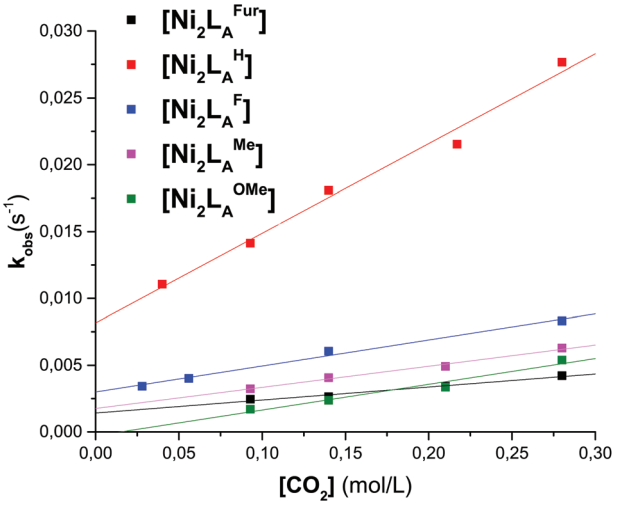

Fig. 3 Plot of k_{obs} *vs.* the CO_2 concentration of L_A^R in MeCN at 298.15 K for the reaction of $[Ni_2L_A^R]$ with CO_2.

cryptand complex. Notably, the CO_2 fixation is slower in $[Ni_2L_A^R](Cl)(ClO_4)_3$ complexes with sterically more bulky groups according to $L^H > L^F > L^{OMe} > L^{Me} \ggg L^{tBu}$. In addition, the application of the furan linker molecules results in a significant decrease of the rate of CO_2 uptake. This kinetic trend is valid for all temperatures measured (Tables S2 and S3†). The small $\Delta H^{\ddagger}$ and $\Delta S^{\ddagger}$ values obtained from the Eyring-plots indicate that the coordination of CO_2 in all substrates proceeds in more than one step.[23] Therefore these small values reflect a more complex association of CO_2 and thus pre-equilibrium and activation enthalpies compose the apparent $\Delta G^{\ddagger}$ value. Comparable changes of the reaction rates upon alteration of the reactive site environment were previously reported by Holm and co-workers on $[Ni^{II}(pyN_2^{R2})(OH)]^-$.[31] In contrast, we present an example that exhibits no obvious alteration of the steric bulk on the metal center.

Azide fixation

A likely explanation for the alteration of the CO_2 uptake kinetics is a decisive change of the Ni–Ni distance and cavity size due to the influence of the linker. A similar hypothesis was reported by Nelson and co-workers.[32] Likewise, the particular shape of the formed HCO_3^- anion can play a significant part in the destabilization within the dinickel complex as one C–O bond is directed towards the opening of the cavity and can interfere with the ligand periphery. As such, the uptake of linear molecules, *e.g.* azides, should not be dramatically influenced by the alteration of the substitution pattern. Along this line we and others have shown structural evidence for the successful azide coordination into the cavity of L_A^R.[9–11,23] Even when no CO_2 binding was observed, such complexes, *e.g.* $[Ni_2L_A^{tBu}](Cl)(ClO_4)_3$, allowed for rapid coordination of N_3^- between both nickel atoms. Correspondingly, we tested the capability of $[Ni_2L_A^R](Cl)(ClO_4)_3$ to allow azide coordination. All investigated azacryptands, except $[Ni_2L_A^{OH,Me}](ClO_4)_2$, show fixation of N_3^-, which is obvious from the changes in their UV-vis spectra by the formation of a new common absorption band at about 350 nm (Fig. S12†).[23] Additionally, ESI-MS analysis further confirms the formation of an azide complex and reveals the respective $[Ni_2L_A^R(N_3)]$ mass peaks. Crystals suitable for X-ray crystallography were obtained for $[Ni_2L_A^F(N_3)](ClO_4)_3$ (Fig. 4) and the results confirm the incorporation of N_3^- between the two Ni-centers. It is notable that the Ni–Ni distance (6.275 Å) is significantly larger than in $[Ni_2L_A^H(N_3)](ClO_4)_3$ (6.129 Å) and $[Ni_2L_A^{tBu}(N_3)](ClO_4)_3$ (6.119 Å).[23,33]

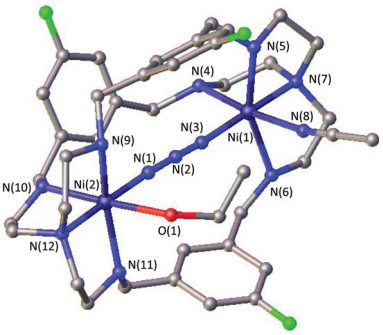

Fig. 4 Molecular structure of $[Ni_2L_A^F(N_3)](ClO_4)_3$. Hydrogen atoms, solvent molecules and counter anions were omitted for clarity.

The general coordination of azides within the cavity and the alteration of the Ni–Ni distances within structurally comparable metal complexes underline the influence of the substitution pattern. It also shows that CO_2 is a key component in the different uptake kinetics. Furthermore, the successful incorporation of negatively charged azides additionally shows that the lone pairs of the furan, pyridine or thiophene linker cannot be a major reason for the weak or no CO_2 binding in $[Ni_2L_A^{Fur}](Cl)(ClO_4)_3$ or $[Ni_2L_A^{Py}](Cl)(ClO_4)_3$, respectively. In light of the acidic properties of CO_2 in an aqueous environment, changes of the substitution pattern might also alter the basicity of the coordinating N-donors and thus the nucleophilicity of the metal atoms. This hypothesis, however, has to be ruled out since the redox potentials of the complexes did not show a trend when electron withdrawing groups (*e.g.* F) or electron donating groups (*e.g.* ^{t}Bu, Me) were installed. For all complexes, multiple irregular electron transfer steps can be observed at ~1.5 V *vs.* Fc/Fc^+, which we were not able to assign (Fig. S13†).

Theoretical analysis

In order to rationalize the experimentally observed differences in CO_2 binding of $[Ni_2L_A^R](Cl)(ClO_4)_3$ complexes, DFT calcu-

lations were performed for complexes with R = H, F, Me and ^{t}Bu (Fig. 5a). Both Ni^{2+} centers were found to be in the high-spin state (S = 1) consistent with the observed octahedral and trigonal-bipyramidal coordinations of the Ni^{2+} centers and this finding is in line with previous SQUID measurements.[23] The two triplet states were found to be exchange-uncoupled by broken-symmetry calculations. Though the substituents differ in their electron-donating and withdrawing capacities, no electronic effect was observed at the nickel ions as well as at all amines, as became apparent from unchanged Mulliken charges, bond distances and orbital compositions. The latter is in-line with the experimental observation that no clear correlation between the CO_2 uptake kinetics and electron donating capacity of the substituent could be found.

However, a noticeable steric effect was observed in the calculations in that rotation of the phenyl groups leads to a steric clash with the bulky ^{t}Bu-substituent (Fig. 5b) while the smaller CH_3 groups allow larger rotational flexibility of the ligand. For R = H and F, the phenyl rotation is essentially unhindered (Fig. 5c).

The bulkiness and flexibility of the substituent correlates with the observed CO_2 uptake kinetics, suggesting that these two factors help in tuning the kinetics and that it is most likely the rate-determining step in the reaction mechanism. Moreover, since the electronic structure at the nickel centers and the amines are the same for all of the complexes, every complex should in principle be able to take up and convert CO_2. This was tested by performing an additional calculation in which Cl^- and MeCN solvent molecules were removed, hydroxide was inserted at the position where the crystal structure contains a H_2O molecule and CO_2 was introduced near the Ni-ions. Geometry optimization indeed leads to a barrier-less formation of HCO_3^- with the driving force being C–O bond formation. An intermediate structure of this mechanism is shown in Fig. 5d, which is in agreement with the mechanism proposed for copper cryptates.[19] Of note here is that contrary to the experimental findings, the Ni–Ni distance is largely independent of the substituent and ranges from 6.09 to 6.11 Å and the starting position of CO_2 has to be chosen such that the Ni–O bond is short and amounts to 2.2 Å. A starting structure with a longer Ni–O distance does not lead to the formation of HCO_3^-. It may thus be conceivable that the different flexibility and dynamics related to the size of the ligand ($\mathbf{L_A^H} < \mathbf{L_A^F} < \mathbf{L_A^{Me}} \lll \mathbf{L_A^{tBu}}$) modulates the initial binding of CO_2 and thereby the Ni–O bond distance as well as the activation and the kinetics towards C–O bond formation. Contrary to the fixation of CO_2, DFT calculations for the fixation of N_3^- reproduce the experimentally observed difference in the Ni–Ni distance (6.129 Å for $\mathbf{L_A^H}$ and 6.261 Å for $\mathbf{L_A^F}$), which clearly is a consequence of a different geometric arrangement of the phenyl groups caused by different substitution patterns.

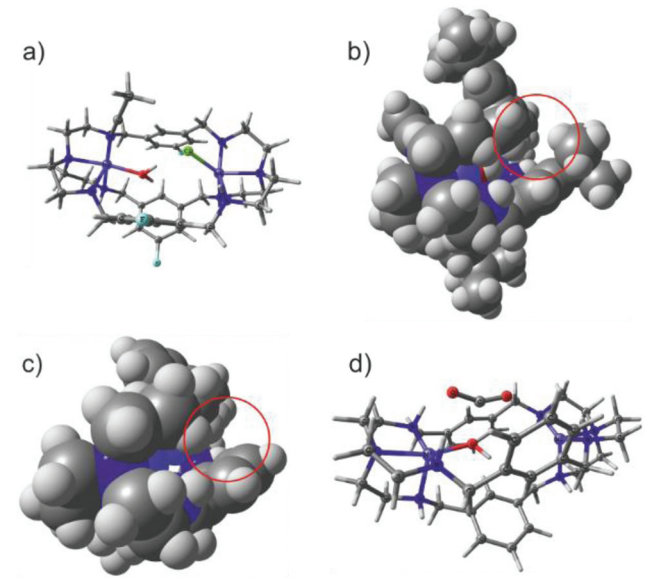

Fig. 5 (a) Geometry optimized structure of $[Ni_2L_A^F]$ with Cl^-, H_2O and MeCN; (b) side view of $[Ni_2L_A^{tBu}]$, showing the steric hindrance of ^{t}Bu with the neighboring phenyl group; (c) side view of $[Ni_2L_A^H]$ where steric effects are absent; (d) intermediate structure with bent CO_2 where CO_2 has been introduced near Ni^{2+} at 2.2 Å, leading to barrierless C–O bond formation towards HCO_3^-.

Conclusion

The coordination of CO_2 in dinickel azacryptands can be manipulated through the presence of different linker molecules comprising Tren cages. UV-vis spectroscopic analyses, as well as ESI-MS analyses clearly show an influence of different functional groups on the CO_2 uptake. Functional groups pointing into the cryptand cavity, as in $\mathbf{L_A^{Fur}}$, $\mathbf{L_A^{Py}}$ or $\mathbf{L_A^{Thio}}$, and $\mathbf{L_A^{OH,Me}}$ significantly slow down or even prohibit a coordination of CO_2. In contrast to this, functional groups pointing out of the cavity show an increasing CO_2-fixation rate with decreasing steric demand ($\mathbf{L_A^{tBu}} \lll \mathbf{L_A^{OMe}} < \mathbf{L_A^{Me}} < \mathbf{L_A^F} < \mathbf{L_A^H}$). Both DFT calculations and cyclic voltammetry demonstrate that there are no electronic effects at the nickel centers as a result of the different substituents. Therefore, we attribute the observed changes in reactivity to structural changes. Furthermore, the DFT calculations performed herein show that with increasing steric demand of the linker, the flexibility of the azacryptand core is decreased, providing a kinetic barrier to the initial coordination of CO_2. In contrast to the binding of CO_2, all dinickel complexes show fixation of azides. The results clearly show that controlling the flexibility of the cryptand can regulate binding of different substrates. With this in hand, new applications might be accessible for azacryptands, *e.g.* within catalysis or gas separation utilizing cryptands as the ligand platform.

Experimental

General techniques

All reactions were performed under either a dry N_2 atmosphere using standard Schlenk techniques or in a glovebox. All

solvents were dried according to standard methods. ^{1}H, ^{13}C NMR spectra were recorded on a Bruker DPX-200 NMR, Bruker DPX-250 NMR or a DPX-400 NMR spectrometer at room temperature. Peaks were referenced to residual ^{1}H signals from the deuterated solvent and are reported in parts per million (ppm). IR spectra were measured with a Bruker Tensor 27 FT-IR spectrometer as a KBr pellet and are reported in cm^{-1}. Mass spectra were measured with a Shimadzu QP-2010 instrument. The dialdehydes[17,34–37] as well as the azacryptands $\mathbf{L_A^{tBu}}$,[17] $\mathbf{L_A^{Fur}}$,[20] $\mathbf{L_A^{Thio}}$,[30] $\mathbf{L_A^{H,para}}$,[26] $\mathbf{L_A^{Py}}$,[20] and $\mathbf{L_I^{OH,Me}}$[31] were synthesized according to literature procedures. All other chemicals were used as received from commercial vendors.

Caution! Perchlorate salts of metal complexes with organic ligands are potentially explosive. They should be handled with care, and prepared only in small quantities.

X-ray data collection and structure solution refinement

Single crystals suitable for X-ray analysis were coated with Paratone-N oil, mounted on a fiber loop, and placed in a cold, gaseous N_2 stream on the diffractometer. $\mathbf{L_I^F}$ and $\mathbf{L_A^{Py}}$ were measured on an Oxford XCalibur diffractometer performing φ and ω scans at 170(2) K. Diffraction intensities were measured using graphite-monochromatic Mo Kα radiation (λ = 0.71073 Å). $\mathbf{[Ni_2L_A^F(N_3)](ClO_4)_3}$, $\mathbf{[Ni_2L_A^{Thio}](ClO_4)_4}$ and $\mathbf{L_A^{OH}}$ were measured on a SuperNova diffractometer performing φ and ω scans at 100(2) K. Diffraction intensities were measured using graphite monochromatic Cu Kα radiation (λ = 1.54184 Å). $\mathbf{[Ni_2L_A^{OH,Me}](ClO_4)_2}$, $\mathbf{L_I^{Me}}$ and $\mathbf{L_I^{OMe}}$ were measured on a STOE IPDS I diffractometer performing ω scans at 170(2) K. Diffraction intensities were measured using graphite-monochromatic Mo Kα radiation (λ = 0.71073 Å). Data collection, indexing, initial cell refinements, frame integration, final cell refinements, and absorption corrections were accomplished with the program CrysAlis Pro (Agilent Technologies, Version 1.171.37.34, 2014) and X-Area, respectively. Space groups were assigned by analysis of the metric symmetry and systematic absences (determined by XPREP) and were further checked by PLATON[38,39] for additional symmetry. Structures were solved by direct methods and refined against all data in the reported 2Θ ranges by full-matrix least squares on F^2 with the SHELXL program suite[40,41] using the OLEX2 interface.[42] The program PLATON SQUEEZE was used for the structures $\mathbf{L_A^{Py}}$ and $\mathbf{[Ni_2L_A^{Thio}](ClO_4)_4}$ to eliminate non-refinable solvent molecules.[43] Crystallographic data as well as refinement parameters are presented in Tables S4–S7 in the ESI.†

Stopped-flow measurements

Time-dependent spectrophotometry was measured with a UV-Vis spectrophotometer S600 from Analytik Jena and a SFA-20 Rapid Kinetics Accessory from Hi-Tech Scientific. Temperature control was obtained with an attached cryostat and a cuvette-holder with a temperature-unit. The used MeCN-solutions were prepared from a stock-solution of MeCN saturated with CO_2 ($[CO_2]_{298K}$ = 0.28 mol L^{-1})[44] and degassed MeCN. The complex was synthesized *in situ* in degassed MeCN under an N_2 atmosphere.

Electrochemical analysis

The electrochemical studies were performed on a Gamry Reference 600 in 100 mM tetrabutylammonium hexafluorophosphate ($TBAPF_6$) as a supporting electrolyte, 20 mM $Ni(ClO_4)_6{\cdot}6H_2O$ and 10 mM $\mathbf{L_A^R}$ in degassed MeCN. Glassy carbon, Pt wire and Ag|$AgNO_3$ (10 mM) in MeCN were used as working, counter and reference electrodes respectively. Cyclic voltammograms (CV) were recorded between −2.0 and +1.5 V at 100 mV s^{-1} in degassed MeCN and after CO_2 purging. The working electrode was polished with alumina paste 0.3 μm (Buehler) before each measurement. The solutions were purged for 10, 20, 60 and 120 seconds with CO_2. The results are reported *versus* Fc/Fc$^+$.

DFT calculations

All calculations have been performed with the ORCA program.[45] The BP86 functional[46] was used along with the Def2-svp basis set.[47] The resolution of the identity (RI) approximation has been employed to speed up the calculation time.[48,49] Scalar relativistic effects are included in zero order regular approach (ZORA).[50,51] Solvent effects were taken into account by using the COSMO solvation model.[52]

General synthetic procedure for $\mathbf{L_I^R}$

In a typical experiment, the respective dialdehyde (3.6 mmol) was dissolved in MeCN (100 mL). A solution of Tren (2.5 mmol) in MeCN (20 mL) was added dropwise to the solution within 3 h. The solution was stirred at RT for 12 h and the formed solid was filtered off, washed with MeCN and dried in a vacuum to give the hexa-imine $\mathbf{L_I^R}$.

$\mathbf{L_I^{OMe}}$: white solid, 85% yield. ^{1}H NMR (400 MHz, $CDCl_3$): δ [ppm] = 7.73 (d, 6H), 7.60 (s, 6H), 5.17 (s, 3H), 3.90 (s, 9H), 3.77 (s, 6H), 3.32 (s, 6H), 2.80 (s, 12H). ^{13}C NMR (100 MHz, $CDCl_3$): δ [ppm] = 160.8, 160.6, 138.4, 125.9, 112.8, 60.1, 56.2, 56.0. ESI-MS calc. for $[C_{39}H_{48}N_8O_3]^+$: m/z = 677.38. Found: m/z = 677.08. IR (KBr, cm^{-1}): 2948, 2875, 2823, 1643, 1590, 1454, 1372, 1197, 1156, 1063, 1030, 863, 697, 657. Anal. calc. for $[C_{39}H_{60}N_8K$ + MeOH + $H_2O]$: N, 15.38; C, 65.80; H, 9.11. Found: N, 15.75; C, 65.73; H, 8.9.

$\mathbf{L_I^{Me}}$: white solid, 85% yield. ^{1}H NMR (400 MHz, $CDCl_3$): δ [ppm] = 8.00 (s, 6H), 7.57 (s, 6H), 5.18 (s, 3H), 3.76 (s, 6H), 3.31 (s, 6H), 3.05–2.62 (m, 12H), 2.54 (s, 9H). ^{13}C NMR (100 MHz, $CDCl_3$): δ [ppm] = 161.2, 139.1, 136.9, 130.2, 128.0, 60.1, 56.1, 21.4. ESI-MS calc. for $[C_{39}H_{49}N_8]^+$: m/z = 629.41. Found: m/z = 629.24. IR (KBr, cm^{-1}): 2947, 2871, 2802, 1641, 1439, 1372, 1333, 1289, 1158, 1068, 1032, 921, 866, 739, 691. Anal. calc. for $[C_{39}H_{48}N_8 + \frac{1}{2}H_2O]$: N, 17.57; C, 73.44; H, 7.74. Found: N, 17.77; C, 73.38; H, 7.75.

$\mathbf{L_I^F}$: white solid, 62% yield. ^{1}H NMR (400 MHz, $CDCl_3$): δ [ppm] = 7.88 (dd, 6H), 7.58 (dd, 6H), 5.30 (s, 3H), 3.73 (s, 6H), 3.32 (s, 6H), 2.80 (s, 12H). ^{13}C NMR (100 MHz, $CDCl_3$): δ [ppm] = 165.0, 162.5, 159.3 (d, J = 2.7 Hz), 139.5 (d, J = 7.4 Hz), 127.8, 114.2, 113.9, 60.0, 55.8. ESI-MS calc. for $[C_{36}H_{40}F_3N_8]^+$: m/z = 641.33. Found: m/z = 641.00. IR (KBr, cm^{-1}): 3070, 2945, 2905, 2885, 2838, 2807, 2734, 1644, 1611, 1432, 1383,

1364, 1287, 1123, 1154, 1067, 1032, 656. Anal. calc. for $[C_{36}H_{39}F_3N_8]$: N, 17.49; C, 67.48; H, 6.14. Found: N, 17.42; C, 67.19; H, 6.26.

$\mathbf{L_I^{OH}}$: yellow solid, 57% yield. ^{1}H NMR (200 MHz, MeOD) δ [ppm]: 7.60 (d, 12H), 5.19 (s, 3H). 3.69 (br s, 3H, OH), 2.73 (m, 12H), 2.56 (m, 12H). ^{13}C NMR (50 MHz, MeOD) δ (ppm): 163.1, 160.8, 139.1, 125.8, 116.1, 60.7, 57.6, 57.1, 40.0. ESI-MS calc. for $[C_{36}H_{44}N_8ONa]^+$: m/z = 659.34. Found: m/z = 659.23. IR (KBr, cm^{-1}): 3352, 2948, 2885, 2832, 1640, 1569, 1435, 1368, 1335, 1240, 1173, 1065, 1024, 924, 876, 733, 692.

General synthetic procedures for $\mathbf{L_A^R}$

The hexa-imine $\mathbf{L_I^R}$ (1.0 mmol) was dissolved in dry MeOH (50 mL) and heated to reflux. KBH_4 (11.7 mmol) was then added in small portions. The reaction mixture was heated under reflux overnight, cooled to RT and the solvent was removed under reduced pressure. The residue was suspended in 2 M NH_4Cl solution (40 mL), extracted with DCM (3 × 40 mL) and dried over $MgSO_4$. The organic solvent was removed under reduced pressure and the remaining solid was dried in a vacuum to give $\mathbf{L_A^R}$.

$\mathbf{L_A^{OMe}}$: white solid, 92%. ^{1}H NMR (400 MHz, $CDCl_3$): δ [ppm] = 6.73 (d, 9H), 4.33 (s, 6H), 3.77 (s, 9H), 3.65 (s, 12H), 2.65 (d, 24H). ^{13}C NMR (100 MHz, $CDCl_3$): δ [ppm] = 159.7, 140.7, 119.9, 113.1, 55.5, 54.5, 53.0, 47.5. ESI-MS calc. for $[C_{30}H_{61}N_8O_3]^+$: m/z = 689.49. Found: m/z = 689.29. IR (KBr, cm^{-1}): 3415, 2944, 2831, 1600, 1462, 1338, 1292, 1160, 1056, 846, 707. Anal. calc. for $C_{39}H_{48}N_8O_3$: N, 16.56; C, 69.21; H, 7.15. Found: N, 16.58; C, 68.88; H, 7.05.

$\mathbf{L_A^{Me}}$: white solid, 99% yield. ^{1}H NMR (400 MHz, $CDCl_3$): δ [ppm] = 7.01 (s, 6H), 6.92 (s, 3H), 3.93 (s, 6H), 3.59 (s, 12H), 2.68 (dd, 24H), 2.27 (s, 9H). ^{13}C NMR (100 MHz, $CDCl_3$): δ [ppm] = 139.5, 138.3, 128.4, 124.7, 54.7, 53.1, 47.6, 21.4. ESI-MS calc. for $[C_{39}H_{619}N_8]^+$: m/z = 641.50. Found: m/z = 641.30. IR (KBr, cm^{-1}): 3443 (br s), 3006, 2919, 2832, 1644, 1607, 1460, 1291, 1162, 1110, 1076, 846, 714. Anal. calc. for $[C_{39}H_{60}KN_8 + \frac{1}{2}H_2O + MeOH]$: N, 15.35; C, 65.80; H, 9.11. Found: N, 15.57; C, 65.73; H, 8.90.

$\mathbf{L_A^F}$: white solid, 99% yield. ^{1}H NMR (400 MHz, $CDCl_3$): δ [ppm] = 6.95 (d, 6H), 6.70 (s, 3H), 3.58 (s, 12H), 2.69–2.59 (m, 24H), 2.03 (s, 6H). ^{13}C NMR (100 MHz, $CDCl_3$): δ [ppm] = 164.3, 161.9, 143.2 (d, J = 7.2 Hz), 122.2, 113.1, 112.9, 55.5, 53.3, 48.0. ESI-MS calc. for $[C_{36}H_{52}F_3N_8]^+$: m/z = 653.43. Found: m/z = 653.20. IR (KBr, cm^{-1}): 3420, 3299, 3075, 2946, 2887, 2818, 1643, 1623, 1453, 1361, 1283, 1149, 1129, 1111, 1000, 788, 662. Anal. calc. for $[C_{36}H_{51}F_3N_8]$: N, 17.16; C, 65.23; H, 7.87. Found: N, 16.95; C, 65.34; H, 7.50.

$\mathbf{L_A^{OH,Me}}$: brown solid, 27% yield. ^{1}H NMR (400 MHz, $CDCl_3$) [ppm]: 6.68 (s, 6H), 3.70 (s, 12H), 2.65 (d, J = 6.4 Hz), 2.156 (s, 9H). ^{13}C NMR (100 MHz, $CDCl_3$): δ [ppm] = 155.6, 129.0, 127.0, 123.8, 54.8, 50.9, 46.8, 20.5. ESI-MS calc. for $[C_{39}H_{61}N_8O_3]^+$: m/z = 689.49. Found: m/z = 689.31, 711.15 [M + Na]$^+$. IR (KBr, cm^{-1}): 3442, 3309, 2964, 2912, 2842, 1735, 1612, 1477, 1262, 1097, 1024, 866, 803, 695. Anal. calc. for $[C_{39}H_{60}N_8K_2O_3 + 4CH_3OH]$: N, 12.52; C, 57.69; H, 8.56. Found: N, 11.93; C, 57.4; H, 8.23.

$\mathbf{L_A^{OH}}$: no extraction with DCM was required. The residue was washed with MeOH and precipitates were filtered off. The solvent was removed under reduced pressure to afford a brownish solid, 84% yield. ^{1}H NMR (200 MHz, MeOD) δ [ppm]: 6.96 (s, 3H), 6.84 (s, 6H), 3.81 (s, 12H), 3.08 (m, 12H), 2.78 (m, 12H). ^{13}C NMR (50 MHz, MeOD) δ [ppm]: 159.3, 138.7, 121.5, 117.0, 53.8, 52.9, 47.7. ESI-MS calc. for $[C_{36}H_{55}N_8O_3]^+$: m/z = 647.43. Found: m/z = 647.45. IR (KBr, cm^{-1}): 3244, 2956, 2836, 1655, 1597, 1456, 1306, 1165, 1101, 1000, 846, 713.

General synthetic procedures for $[Ni_2L_A^R](Cl)_y(ClO_4)_x$ (x = 2–4; y = 0, 1)[23]

The respective compound $\mathbf{L_A^R}$ (0.038 mmol) was dissolved in 2 mL degassed MeCN/MeOH or MeCN/EtOH 4 : 1. A solution of $Ni(ClO_4)_2{\cdot}6H_2O$ (0.078 mmol) in MeCN/EtOH 4 : 1 was added and the mixture was stirred for 12 h at room temperature. The solvent was removed under reduced pressure and the residue was crystallized from MeCN/Et_2O, or through slow evaporation of the solvent.

$\mathbf{[Ni_2L_A^{Me}](Cl)(ClO_4)_3}$: blue solid, 69% yield. ESI-MS calc. for $[C_{39}H_{61}N_8Ni_2 + 3ClO_4]^+$: m/z = 1054.22. Found: m/z = 1054.7. IR (KBr, cm^{-1}): 3421, 2957, 1637, 1613, 1443, 1385, 1146, 1115, 1086, 874, 842, 753, 629.

$\mathbf{[Ni_2L^F](Cl)(ClO_4)_3}$: blue solid, 60% yield. ESI-MS calc. for $[C_{36}H_{51}F_3N_8Ni_2 + CH_3CN]^+$: m/z = 809.32. Found: m/z = 809.3. IR (KBr, cm^{-1}): 3422, 2933, 2875, 1665, 1626, 1598, 1459, 1342, 1300, 1144, 1115, 1085, 982, 878, 841, 664, 628.

$\mathbf{[Ni_2L_A^{OMe}](Cl)(ClO_4)_3}$: green solid, 90% yield. ESI-MS calc. for $[C_{39}H_{55}N_8Ni_2O_3 + 2ClO_4^- + CH_3CN]^+$: m/z = 1038.23. Found: m/z = 1038.4. IR (KBr, cm^{-1}): 3413, 2955, 2843, 1651, 1605, 1467, 1440, 1340, 1302, 1143, 1112, 1084, 842, 710, 627.

$\mathbf{[Ni_2L_A^{Fur}](Cl)(ClO_4)_3}$: green solid, 42% yield. ESI-MS calc. for $[C_{30}H_{49}N_8Ni_2O_3 + 3ClO_4]^+$: m/z = 982.11. Found: m/z = 982.63. IR (KBr, cm^{-1}): 3458, 3250, 2858, 1653, 1450, 1344, 1092, 928, 816, 627.

$\mathbf{[Ni_2L_A^{Py}](Cl)(ClO_4)_3}$: dark blue solid, 98% yield. ESI-MS calc. for $[C_{33}H_{51}N_{11}Ni_2 + CH_3CN]^+$: m/z = 758.33, 1015.16 [+3ClO_4]. Found: m/z = 758.06, 1015.08 [+3ClO_4]. IR (KBr, cm^{-1}): 3418, 1940, 1883, 1641, 1608, 1458, 1143, 1085, 794, 627.

$\mathbf{[Ni_2L_A^{Thio}](ClO_4)_4}$: blue crystals, 26% yield. ESI-MS calc. for $[C_{30}H_{48}N_8Ni_2S_3 + 3ClO_4]^+$: m/z = 1029.0. Found: m/z = 1028.5. IR (KBr, cm^{-1}): 3416 (br), 3256, 3061, 2949, 2835, 1629, 1448, 1294, 1147, 1112, 1088, 1007, 885, 742, 683, 629.

$\mathbf{[Ni_2L_A^{OH}](ClO_4)_3}$: green solid, 87% yield. ESI-MS calc. for $[C_{36}H_{55}Cl_2N_8Ni_2O_7]^+$: m/z = 897.22. Found: m/z = 896.8. IR (KBr, cm^{-1}): 3387, 3230, 2965, 2781, 1642, 1603, 1460, 1310, 1140, 1086, 995, 628.

$\mathbf{[Ni_2L_A^{OH,Me}](ClO_4)_2}$ was obtained by crystallization from MeCN. Blue crystals, 13% yield. ESI-MS calc. for $[C_{39}H_{59}N_8Ni_2O_3]^+$: m/z = 803.35. Found: m/z = 803.25. IR (KBr, cm^{-1}): 3422, 3272, 2919, 2808, 1637, 1473, 1309, 1261, 1085, 954, 821, 626.

Acknowledgements

This work was supported by the Fonds der Chemischen Industrie (Liebig grant to U.-P. A.) and through the Deutsche Forschungsgemeinschaft (Emmy Noether grant to U.-P. A., AP242/2-1) as well as the Max Planck Gesellschaft (M. v. G.). F. M. gratefully acknowledges financial support by the Deutsche Bundesstiftung Umwelt. We thank Prof. Christian Herrmann, Physical Chemistry, Ruhr-University Bochum, for providing the stopped flow equipment and for valuable discussions. Open Access funding provided by the Max Planck Society.

Notes and references

1 V. Begoña and S. B. Salvador, *Eur. J. Inorg. Chem.*, 2008, **1**, 84–97.
2 C. E. Wilmer, O. K. Farha, Y.-S. Bae, J. T. Hupp and R. Q. Snurr, *Energy Environ. Sci.*, 2012, **5**, 9849–9856.
3 J. Fu, S. Das, G. Xing, T. Ben, V. Valtchev and S. Qiu, *J. Am. Chem. Soc.*, 2016, **138**, 7673–7680.
4 Y. Zeng, R. Zou and Y. Zhao, *Adv. Mater.*, 2016, **28**, 2855–2873.
5 J. Jaschik, M. Jaschik and K. Warmuziński, *Chem. Process Eng.*, 2016, **37**, 29–39.
6 M. Tong, Q. Yang and C. Zhong, *Microporous Mesoporous Mater.*, 2015, **210**, 142–148.
7 E. S. Sanz-Pérez, C. R. Murdock, S. A. Didas and C. W. Jones, *Chem. Rev.*, 2016, **116**, 11840–11876.
8 Y. Jia, H. Su, Z. Wang, Y.-L. E. Wong, X. Chen, M. Wang and T. W. D. C. Chan, *Anal. Chem.*, 2016, **88**, 9364–9367.
9 L. Fabbrizzi, P. Pallavicini, L. Parodi, A. Perotti, N. Sardone and A. Taglietti, *Inorg. Chim. Acta*, 1996, 7–9.
10 M. G. Drew, J. Hunter, D. J. Marrs, J. Nelson and C. Harding, *J. Chem. Soc., Dalton Trans.*, 1992, 3235–3242.
11 C. J. Harding, F. E. Mabbs, E. J. L. MacInnes, V. McKee and J. Nelson, *J. Chem. Soc., Dalton Trans.*, 1996, 3227–3230.
12 M. G. Basallote, J. Durán, M. J. Fernández-Trujillo and M. A. Máñez, *J. Chem. Soc., Dalton Trans.*, 2002, 2074–2079.
13 J.-M. Lehn, *Pure Appl. Chem.*, 1980, **11**, 2442–2459.
14 J. M. Lehn, *Pure Appl. Chem.*, 1978, **50**, 871–892.
15 V. Amendola, L. Fabbrizzi, C. Mangano, P. Pallavicini and M. Zema, *Inorg. Chim. Acta*, 2002, **337**, 70–74.
16 V. Amendola, M. Bonizzoni, D. Esteban-Gómez, L. Fabbrizzi, M. Licchelli, F. Sancenón and A. Taglietti, *Coord. Chem. Rev.*, 2006, **250**, 1451–1470.
17 A. A. C. Wild, K. Fennell, G. G. Morgan, C. M. Hewage and J. P. G. Malthouse, *Dalton Trans.*, 2014, **43**, 13557.
18 P. Mateus, R. Delgado, V. André and M. T. Duarte, *Inorg. Chem.*, 2015, **54**, 229–240.
19 M. M. El-Hendawy, S. Bandaru, N. J. English and D. A. Mooney, *Catal. Sci. Technol.*, 2013, **3**, 2234–2243.
20 Y. Dussart, C. Harding, P. Dalgaard, C. McKenzie, R. Kadirvelraj, V. McKee and J. Nelson, *J. Chem. Soc., Dalton Trans.*, 2002, 1704–1713.
21 J.-M. Chen, W. Wei, X.-L. Feng and T.-B. Lu, *Chem. – Asian J.*, 2007, **2**, 710–719.
22 F. Arnaud-Neu, S. Fuangswasdi, B. Maubert, J. Nelson and V. McKee, *Inorg. Chem.*, 2000, **39**, 573–579.
23 F. Möller, K. Merz, C. Herrmann and U.-P. Apfel, *Dalton Trans.*, 2016, **45**, 904–907.
24 P. J. Cragg, *A Practical Guide to Supramolecular Chemistry*, Wiley-VCH, England, 2005.
25 R. M. Town, V. McKee, M. Arthurs and J. Nelson, *J. Chem. Educ.*, 2001, **78**, 1269.
26 D. Chen and A. E. Martell, *Tetrahedron*, 1991, **47**, 6895–6902.
27 M. F. Mahon, J. McGinley, A. Denise Rooney and J. M. D. Walsh, *Inorg. Chim. Acta*, 2009, **362**, 2353–2360.
28 J. Nelson, V. McKee and G. G. Morgan, *Prog. Inorg. Chem.*, 1998, **47**, 167–316.
29 M. G. Drew, C. J. Harding, O. W. Howarth, Q. Lu, D. J. Marrs, G. G. Morgan, V. McKee and J. Nelson, *J. Chem. Soc., Dalton Trans.*, 1996, 3021–3030.
30 T. Lu, X. Zhuang, Y. Li and S. Chen, *J. Am. Chem. Soc.*, 2004, **15**, 4760–4761.
31 D. Huang, O. V. Makhlynets, L. L. Tan, S. C. Lee, E. V. Rybak-Akimova and R. H. Holm, *Inorg. Chem.*, 2011, **50**, 10070–10081.
32 V. McKee, J. Nelson and R. M. Town, *Chem. Soc. Rev.*, 2003, **32**, 309–325.
33 A. Escuer, C. J. Harding, Y. Dussart, J. Nelson, V. McKee and R. Vicente, *J. Chem. Soc., Dalton Trans.*, 1999, 223–228.
34 R. P. Jimenez, M. Parvez, T. C. Sutherland and J. Viccars, *Eur. J. Org. Chem.*, 2009, 5635–5646.
35 F. Banishoeib, A. Henckens, S. Fourier, G. Vanhooyland, M. Breselge, J. Manca, T. J. Cleij, L. Lutsen, D. Vanderzande, L. H. Nguyen, H. Neugebauer and N. S. Sariciftci, *Thin Solid Films*, 2008, **516**, 3978–3988.
36 J. Bao, Z. Zhang, R. Tang, H. Han and Z. Yang, *J. Lumin.*, 2013, **136**, 68–74.
37 X.-Y. Yang, W. S. Tay, Y. Li, S. A. Pullarkat and P.-H. Leung, *Organometallics*, 2015, **34**, 1582–1588.
38 A. L. Spek, *J. Appl. Crystallogr.*, 2003, **36**, 7–13.
39 A. L. Spek, *Acta Crystallogr., Sect. D: Biol. Crystallogr.*, 2009, **65**, 148–155.
40 G. M. Sheldrick, *Acta Crystallogr., Sect. A: Fundam. Crystallogr.*, 2008, **64**, 112–122.
41 C. B. Hübschle, G. M. Sheldrick and B. Dittrich, *J. Appl. Crystallogr.*, 2011, **44**, 1281–1284.
42 O. V. Dolomanov, L. J. Bourhis, R. J. Gildea, J. A. K. Howard and H. Puschmann, *J. Appl. Crystallogr.*, 2009, **42**, 339–341.
43 A. L. Spek, *Acta Crystallogr., Sect. C: Cryst. Struct. Commun.*, 2015, **71**, 9–18.
44 A. Gennaro, A. A. Isse and E. Vianello, *J. Electroanal. Chem.*, 1990, **289**, 203–215.
45 F. Neese, *Wiley Interdiscip. Rev.: Comput. Mol. Sci.*, 2012, **2**, 73–78.
46 A. D. Becke, *Phys. Rev. A*, 1988, **38**, 3098–3100.

47 D. A. Pantazis, X.-Y. Chen, C. R. Landis and F. Neese, *J. Chem. Theor. Comput.*, 2008, **4**, 908–919.
48 K. Eichkorn, O. Treutler, H. Öhm, M. Häser and R. Ahlrichs, *Chem. Phys. Lett.*, 1995, **240**, 283–290.
49 K. Eichkorn, F. Weigend, O. Treutler and R. Ahlrichs, *Theor. Chem. Acc.*, 1997, **97**, 119–124.
50 E. van Lenthe, A. van der Avoird and P. E. S. Wormer, *J. Chem. Phys.*, 1998, **108**, 4783–4796.
51 E. van Lenthe, J. G. Snijders and E. J. Baerends, *J. Chem. Phys.*, 1996, **105**, 6505–6516.
52 A. Klamt and G. Schüürmann, *J. Chem. Soc., Perkin Trans. 2*, 1993, 799–805.